

Assessment of Organobentonite's Adsorption Kinetics for Efficient Removal of Methylene Blue Dye from Aqueous Solutions

Sami Mohammad¹, Mohamad Nasir Mohamad Ibrahim¹, Sumiyyah Sabar², Rahadian Zainul^{3*},
Ida Ayu Gede Widihati⁴, Harits Atika Ariyanta⁵ and Anwar Iqbal^{1*}

¹School of Chemical Sciences, Universiti Sains Malaysia, 11800 USM, Penang, Malaysia

²Chemical Science Programme, School of Distance Education, Universiti Sains Malaysia, 11800 Minden, Penang, Malaysia

³Department of Chemistry, Faculty of Mathematics and Natural Sciences, Universitas Negeri Padang, Indonesia

⁴Chemistry Department, Faculty of Mathematics and Natural Science, Udayana University, Indonesia

⁵Research Center for Biomass and Bioproducts, National Research and Innovation Agency (BRIN), Jl Raya Bogor KM 46, Cibinong 16911, Indonesia

*Corresponding author (e-mail: anwariqbal@usm.my; rahadianzmsiphd@fmipa.unp.ac.id)

Organobentonite beads (CS/SA/SS/Ben-300 mg) were synthesised using the ionic gelation method by crosslinking bentonite (Ben), chitosan (CS), sodium alginate (SA) and sodium sulphate (SS). The synthesised beads were characterised using X-ray diffraction (XRD), Fourier-transform infrared (FTIR) spectroscopy and a digital microscope, which indicated successful crosslinking between the components. The batch adsorption method was employed to investigate the adsorptive capabilities of CS/SA/SS/Ben-300 mg using methylene blue (MB) as a dye model. The highest adsorption of MB (50 mg/L) (88%) followed the pseudo-second-order kinetic model with a rate constant of 0.9195 g mg⁻¹ min⁻¹ and a linear regression coefficient (R²) of 0.98 at 323 K and pH 12. This suggests that the MB adsorption followed a chemisorption mechanism. Furthermore, the Langmuir model was found to better describe the adsorption process compared to the Freundlich model. According to the Langmuir isotherm, the maximum monolayer adsorption capacity (q_{max}) of the organobentonite beads was observed to be 48.94 mg/g under the optimum conditions. The reusability of CS/SA/SS-Ben-300 mg demonstrated no significant decrease in MB removal efficiency.

Keywords: Adsorption; bentonite; chitosan; methylene blue; sodium alginate; sodium sulphate

Received: October 2023; Accepted: February 2024

The global consumption of textile products has increased dramatically over the last decades. The worldwide textile industry is estimated to produce between 100 and 150 billion textiles annually [1]. The expansion of textile industries has resulted in the generation of a massive amount of wastewater contaminated with dyes. In the dyeing process, only 10% of the dyes remain on the fabric, whereas 90% will be discharged as effluent [2]. The effluents typically comprise a mixture of multiple dyes in varying percentages, depending on the extent of the dye employed in industry, mixing ratios, and concentration levels [3]. The majority of the dyes used in textile industries are unaffected by light, biodegradation and oxidation processes due to their complex aromatic structure. The presence of these dyes in the ecosystem has been identified to be toxic [2].

Several methods for removing synthetic dyes from wastewater have been developed to reduce their environmental impact. Decolourisation has been accomplished by using several remediation strategies, such as photocatalytic oxidation, microbiological or biodegradation, and adsorption on various organic or

inorganic matrices [4-6]. The adsorption technique offers numerous advantages, including flexibility, ease of design, cost-effectiveness, simplicity of operation, and the ability to regenerate [7]. Extending the repertory of adsorbents with natural materials such as clays appears promising due to their effectiveness and affordability [8]. The surface of clays contains several surface-active sites, such as Brønsted and Lewis acid sites and ion exchange sites. These sites caused the clays to have very selective preferences towards certain dyes [9]. Clays, in their natural form, have limited adsorption capability. Reports have shown that modifying clays with organic and inorganic modifiers can improve their properties.

Shahinpour et al. [10] developed a magnetic bio-based κ -carrageenan-kaolinite hydrogel adsorbent to remove Congo red and Alizarin red dyes. The maximum adsorption capacities of Congo red and Alizarin red were 26.9 mg/g and 33.5 mg/g, respectively. The adsorption process is driven by π - π stacking, electrostatic interaction, dipole-dipole H bonding, and Yoshida H bonding. The presence of magnetic properties also allows the adsorbent to be separated easily. In a

separate research, Marrakchi et al. [11] synthesised epichlorohydrin crosslinked chitosan/carbon-clay biohybrid adsorbent for the adsorption of cationic methylene blue and anionic azo acid blue 29. The adsorption capacity was 86.08 mg/g for MB and 132.04 mg/g for AB 29 at 30 °C. Khan et al. [12] prepared a three-dimensional (3D) amphoteric composite aerogel from dodecyl amine-modified kaolinite enriched chitosan/alginate for the adsorption of anionic and cationic dyes. The adsorption capacities towards methylene blue and acid black were around 73.1 and 71.5 mg/g, respectively. The adsorption mechanism was identified to be via electrostatic interaction.

Chitosan and alginate are biopolymers that are compatible to be crosslinked among themselves and with other crosslinkers, including clays. Aside from its excellent biocompatibility and biodegradability, chitosan and alginate are distinguished by their accessibility, low cost, non-toxicity, antibacterial activity, and simplicity of modification [13-15]. However, chitosan and alginate individually cannot effectively remove dyes due to the formation of colloids in water, degradation by chemical actions and low surface area [16]. Chitosan and alginate are often crosslinked to improve their properties and form amphoteric adsorbent. Regardless, this composite material is prone to mechanical weakness [17].

Hence, this work explores the feasibility of organobentonite beads prepared by crosslinking chitosan and alginate with bentonite for the adsorption of methylene blue. Chitosan and sodium alginate are known to swell when in contact with water; this condition can sometimes hamper adsorption. To control the degree of swelling, sodium sulphate was added. Sodium sulphate can disrupt the interactions between chitosan and sodium alginate through crosslinking and restrict the affinity of chitosan/

sodium alginate to water. In addition, the sodium sulphate also provides extra sites for dye adsorption [18]. Bentonite is a type of clay composed primarily of montmorillonite, an expandable layered aluminosilicate mineral. Each layer is composed of two silicate tetrahedral sheets, sandwiching one aluminate octahedral sheet. The aluminosilicate layers have permanent negative charges on their surfaces, which are compensated by inorganic cations such as Na^+ and Ca^{2+} [19]. These cations can be replaced with cation biopolymers such as chitosan. The beads were thoroughly characterised to understand the physicochemical and adsorption properties.

MATERIALS AND METHODOLOGY

Chemicals and Materials

Chitosan used in this study was purchased from Dober Chemical Ltd., USA. It had a deacetylation degree of 91% and an average molecular weight of approximately 310,000 g/mol. Bentonite (MW~360.31 g/mol) was purchased from R&M Chemicals. Methylene blue (MB) was obtained from Sigma-Aldrich Chemicals. Other chemicals include analytical grade acetic acid (ASC, Macron, 95–97 %), sodium alginate (Sigma-Ald, S2252, 99 %), calcium chloride (Sinopharm Chem. Reagent Co., Ltd.), sodium sulphate (Merck Chemicals), and sodium hydroxide (Sigma Aldrich, S2252, 99 %). All the chemicals were analytical-grade and required no additional purification.

Synthesis of Organobentonite Beads

The synthesis procedure was adopted from Yang et al. [20]. Briefly, 50 mg of chitosan (CS) was dissolved in 50 mL of 1.0% (v/v) acetic acid, which resulted in 0.1% (w/v) CS solution. Thereafter, 12.5 mg of sodium sulphate (SS) was added to the CS solution with continuous stirring for 2 hours.

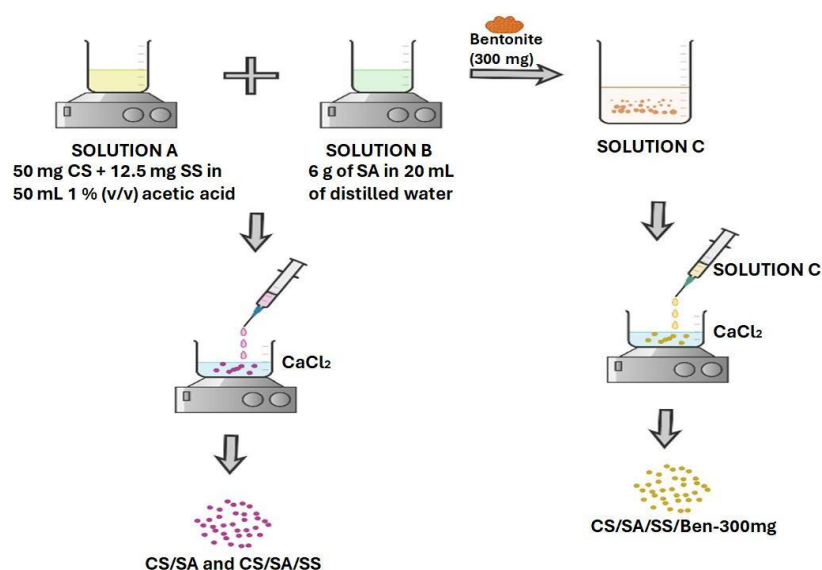


Figure 1. The schematic presentation of the organobentonite beads synthesis.

This solution was assigned as Solution A. Sodium alginate (SA) solution with a weight-to-volume ratio of 3 % was prepared by mixing 6 g of SA with 200 mL of distilled water and stirred for 3 hours. This solution was assigned as Solution B. Next, Solutions A and B were thoroughly mixed, followed by the addition of 300 mg bentonite (Ben). The mixture was stirred for 3 hours (Solution C). The beads were prepared by dropping Solution C into a calcium chloride solution (0.30 M). The beads were stirred for 30 minutes in the calcium chloride solution before being separated, rinsed with distilled water and air-dried for 24 hours. Beads without sodium sulphate (CS/SA) and without bentonite (CH/SA/SS) were prepared in a similar manner for comparison. The CS/SA and CH/SA/SS were not characterised. The beads with 300 mg of Ben were labelled as CS/SA/SS/Ben-300 mg. The preparation process is simplified in Figure 1.

Characterisations of the Prepared Organobentonite Beads

The concentration of MB was determined using UV-visible (Shimadzu UV 1800; Germany) at a wavelength of 664 nm. The attenuated total reflectance Fourier transform infrared spectroscopy (ATR-FTIR) (Perkin Elmer model System 2000; USA), was used to determine the functional groups. The crystallinity of the beads was analysed using X-ray diffraction (XRD; model PANalytical X'pert Pro MRD PW 603040/60). A Cu tube was used as the x-ray generator with a wavelength of 1.5406 Å at 40 kV and 40 mA. The XRD patterns were recorded in the range of 5 to 80°. The photograph image of the beads and the diameter were determined using a digital microscope (VHX-7000; USA).

Batch Adsorption Experiments

The adsorption experiment was carried out using 50 mL of MB solution which was continuously stirred throughout the study. The absorbance of MB at different periods was determined using a Shimadzu UV-1800 spectrophotometer at 664 nm. The MB removal percentage was calculated using the equation 1:

$$\text{Percent removal (\%)} = \frac{C_o - C_e}{C_o} \times 100 \quad (1)$$

where C_o and C_e represent the MB concentration at the initial and equilibrium state (mg/L), respectively. The amount adsorbed at equilibrium, q_e (mg/g) was determined according to equation 2:

$$q_e = \frac{(C_o - C_e)V}{m} \quad (2)$$

where C_o is the dye concentration before adsorption (mg L⁻¹); C_e represents the dye concentration at

equilibrium (mg L⁻¹); V is the volume of the MB solution (L), and m is the mass of the adsorbent used (g).

Effect of pH

The effect of initial pH on the adsorption of MB was studied at pH 3, 5, 7, 10 and 12, at a constant temperature of 303 K. The initial pH of the MB solution was adjusted using 0.10 M HCl or NaOH. The study used 100 mg of beads with an initial MB concentration of 50 mg/L, 50 ml for 4 h.

Effect of Initial MB Concentration

The effect of initial MB concentration was studied at 50, 100, 150, 200, 250, and 300 mg/L. The pH of the solution was maintained at pH 12 using 100 mg of adsorbent for 4 hours.

Effect of Contact Time

The effect of contact time was studied at a time range of 1, 2, 3, 4, 5 and 6 hours. The MB concentration was maintained at 50 mg/L, volume of 50 mL with 100 mg of adsorbent. The pH was maintained at pH 12.

Effect of Adsorbent Dose

The effect of adsorbent dosage was studied using 100 mg, 200 mg, 300 mg, 400 mg, 500 mg and 600 mg. The MB concentration and volume were 50 mg/L and 50 mL, respectively at pH 12 for 6 hours.

Effect of Temperature

The effect of temperature was studied at 303 K, 313 K and 323 K. The pH was maintained at pH 12. The initial MB concentration and volume used were 50 mg/L and 50 ml. The beads dosage used was 400 mg for 6 h.

Regeneration of Adsorbent

Desorption experiments were performed to investigate the potential of CS/SA/SS/Ben-300 mg re-generation. The MB-loaded beads were added to 50 mL of 0.1 M HCl as the desorbing solution. The adsorbent was separated after 8 hours of shaking at room temperature, and the quantity of MB desorbed (D, %) was calculated using equation 3:

$$D = \frac{C_{des}}{C_{ads}} \times 100 \quad (3)$$

where C_{des} and C_{ads} are the amounts of MB desorbed and adsorbed, respectively. The beads were washed with water after each cycle of adsorption and desorption before being reused. Three sequential adsorption-desorption cycles were performed.

Determination pH of Point of Zero Charge (pH_{PZC})

To calculate the pH_{PZC} , the initial pH (pH_i) of 100 mL of distilled water was adjusted with either 0.1 M HCl or NaOH to a range of values from pH 3 to pH 12. After that, 100 mg of the beads were added to the solutions. After shaking the dispersions at a temperature of 303 K for 2 days, the final pH of the solutions (pH_f) was determined. The pH_{PZC} value was determined by finding the point on the graph where the curve of pH_f vs. pH_i intersected with the line, indicating that $pH_f = pH_i$.

RESULTS AND DISCUSSION

Characterisation of Adsorbents

The digital photograph of CS/SA/SS and CS/SA/SS/Ben-300 mg beads captured are presented in Figure 2(a). The diameter of CS/SA/SS and CS/SA/SS/Ben-300 mg beads was measured to be 3672.5 μm and 3879.5 μm , respectively. The bentonite could have prevented the beads from shrinking during the drying process, resulting in a higher diameter.

The FT-IR spectra of CS/SA, CS/SA/SS and CS/SA/SS/Ben-300 are shown in Figure 2(b). The bands around 1019 cm^{-1} correspond to (CO-C) stretching of the saccharide structure of sodium alginate (SA). The broad peak around 3295 cm^{-1} corresponds to the OH and NH₂ stretching vibration. The peak around 1600 cm^{-1} is attributed to the stretching vibration of C=O of SA and the residual N-acetyl groups (CO- extension of amide I) of CS. The peak around 1410 cm^{-1} appeared in response to the stretching vibration of COO- groups in SA. The weak bands around 830-1400 cm^{-1} in chitosan are typically attributed to C-N stretching of amide III, C-O-C deformation, C-O stretching, and C-O and free amine group [21]–[23]. These peaks appear to be broader in the spectrum of CS/SA/SS, suggesting possible overlapping with the sulphate group [24]–[26]. The typical FTIR peaks related to the bentonite, namely at 467 cm^{-1} , 517 cm^{-1} , 783 cm^{-1} , 1120 cm^{-1} , 1034 cm^{-1} and 1634 cm^{-1} for Si-O-Si of quartz, 617 cm^{-1} and 675 cm^{-1} referring to Al-O-Si-O bond and Al-Al-OH bond at 917 cm^{-1} could distinctly identified due to overlapping with functional groups such as functional groups of -OH, C-O and C=O.

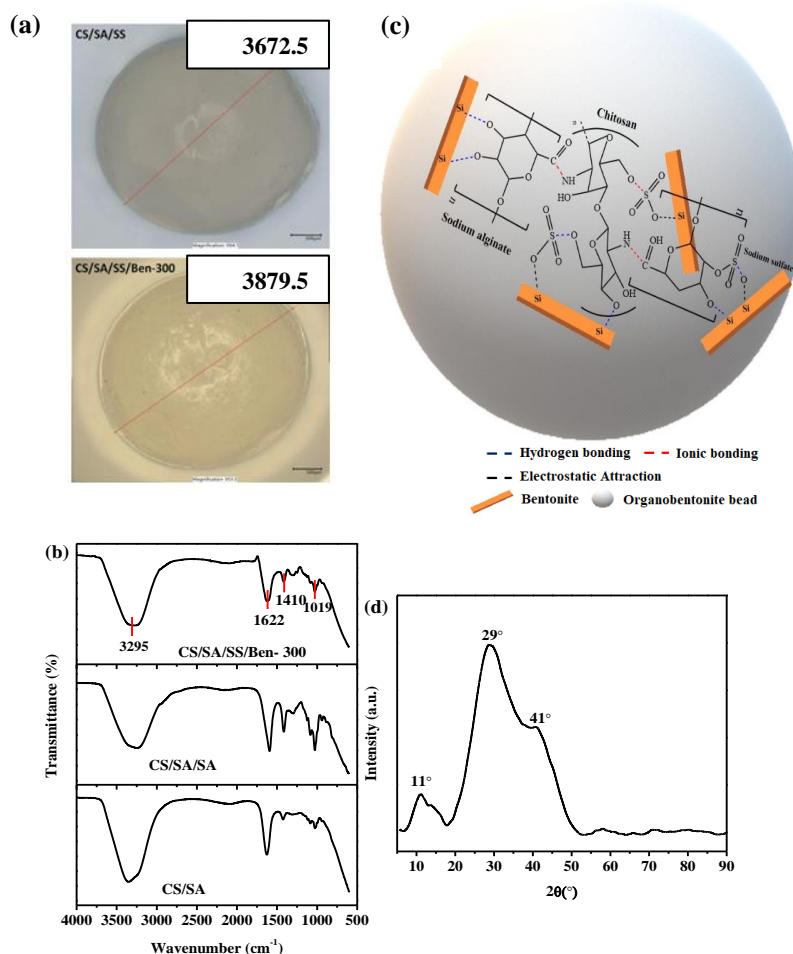


Figure 2. (a) The digital photograph of CS/SA/SS and CS/SA/SS/Ben-300 mg beads (b) The FTIR spectrum of the prepared beads, (c) schematic diagram representing the interaction among the components in CS/SA/SS/Ben-300 mg and (d) the XRD diffractogram of CS/SA/SS/Ben-300 mg.

Possible Crosslinking between Chitosan, Sodium Alginate, Sodium Sulphate and Bentonite

The FTIR analysis indicates that the reactants used contain abundant functional groups that can act as adsorption sites. The CS can interact with negatively charged groups of (Si-O) by electrostatic interactions, while hydrogen bonding also develops between bentonite and the CS/SA components. The ion exchange interaction between sodium sulphate and bentonite occurs by replacing the exchangeable cations in the clay, such as Ca^{2+} and Mg^{2+} in bentonite, with Na^+ from the sulphate salt [27]. The schematic diagram representing the interactions is shown in Figure 2(c).

The XRD diffractograms of CS/SA/SS/Ben-300 mg adsorbent is presented in Figure 2(d). The XRD peak around $2\theta = 29^\circ$ and a shoulder at $2\theta = 11^\circ$ and 41° are attributed to the (200) plane from polymannuronate, (110) plane from polyguluronate unit and other from amorphous halo, respectively of sodium alginate [28]. The XRD diffraction peaks at $2\theta = 11^\circ$ and 41° can be associated with chitosan as well. The broadness of these peaks indicates the interaction between the components is so strong that it affect the hydrogen bonding within the chitosan framework and eventually changes the crystallinity of the chitosan to amorphous [29-31]. The XRD diffraction peaks of pure bentonite were not observed due to the low amount of bentonite used.

1. Adsorption of Methylene Blue

Influence of pH

The pH of a solution influences the surface charge of the adsorbent and the ionisation form of the pollutants [32]. The pH studied was within pH 3 to 12 with the initial concentration of 50 mg/L for 4 h and the adsorption profile is shown in Figure 3(a). The adsorption percentage was observed to increase as the pH increased. Highest removal was achieved at pH 12 (73%), whereas the lowest adsorption was achieved at pH 3 (56%). The pH_{PZC} (Figure 3(b)) of the adsorbent was determined to be 5.6. Above this pH, the surface of the adsorbent will be negatively charged as a consequence of the presence of hydroxide ions (OH^-), and readily absorb the cationic MB species onto its surface via electrostatic attraction [33]. Also, the deprotonation of the $-\text{NH}_3^+$ and $-\text{OH}_2^+$ functional groups took place above the pH_{PZC} , increasing the attraction towards the adsorbent. On the other hand, when the pH of the solution is less than pH 7, the surface of the adsorbent exhibits a positive charge, leading to an electrostatic repulsion between the MB cations and the adsorbent. Such a repulsion leads to a lower adsorption efficiency [34]. Also, the high concentration of H^+ ions at low pH levels competes with dye cations for surface active sites [35]. In addition, the amino groups in CS and carboxylic acid groups in SA are protonated at acidic pH, creating a positively charged surface on the adsorbent [36].

Based on the adsorption percentage, pH 12 was chosen as the optimum pH to optimise other parameters.

Influence of Initial MB Concentration

The influence of initial MB concentration on the adsorption of MB was tested at pH 12 in the range of 50-300 mg/L for 4 hours. From Figure 3(c), the adsorption of MB can be seen as dependent on the initial concentration of MB solution. The adsorption of MB decreased as the initial concentration decreased. The highest removal of 73% was obtained at 50 mg/L, whereas the lowest removal was obtained at 300 mg/L. A lower adsorption percentage was achieved at a higher concentration due to the limited vacant adsorption sites. The repulsion among the MB molecules at higher concentrations can also lead to lower adsorption [37]. Whereas at lower concentrations, the ratio of the vacant adsorption sites compared to MB is higher, permitting faster and higher adsorption. The initial concentration of 50 mg/L was considered as the optimum MB concentration and was used for the optimisation of other parameters.

2. Influence of Contact Time

The influence of contact time on the adsorption of MB is shown in Figure 3(d). The investigation was carried out using 50 mg/L MB at pH 12. The adsorption of MB was rapid at the initial stage due to the availability of vacant adsorption sites and higher MB concentration. As time progressed, the adsorption gradually slowed due to fewer available vacant adsorption sites and lower MB concentration [38, 39]. Highest adsorption was achieved at 6 hours (80%); hence it was used as the optimum time.

3. Influence of Adsorbent Dosage

The influence of adsorbent dosage on the MB adsorption is shown in Figure 3(e). The adsorption of MB increased from 78% to 87% when the dosage was increased from 100 mg to 400 mg. Further increase did not result in changes. Hence, 400 mg is taken as the optimum dosage.

Influence of Temperature

The adsorption process is known to be significantly influenced by temperature. Generally, when temperature increases, the adsorbate will obtain extra energy to interact with the adsorbent surface. The influence of temperature on the MB adsorption was investigated at 303 K, 313 K and 323 K. As shown in Figure 4(f), the maximum adsorption of MB (88%) was achieved at 323 K. At this temperature, the adsorbent surface's kinetic energy and the dye molecules' kinetic energy are high. This causes a faster transfer of mass and increases the amount of contact between the dye molecules and the adsorbent, all of which point to an endothermic character to the adsorption of MB on the surface of the beads.

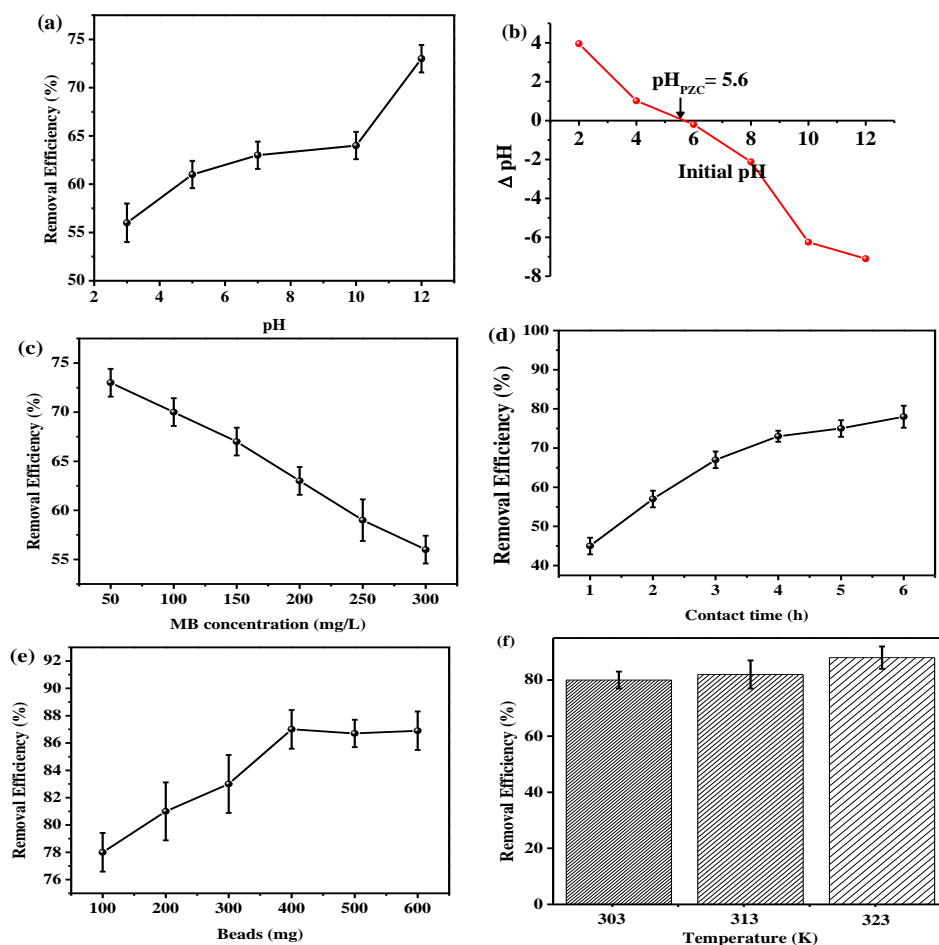


Figure 3. The influence of (a) pH (b) point of zero charge (pHpzc) (c) initial MB concentrations (d) contact time (e) adsorbent dosage and (f) temperature on the adsorption of MB.

Based on the collected data, the optimum conditions were 400 mg CS/SA/SS/Ben-300 mg, initial MB concentration of 50 mg/L MB at pH 12 for 6 hours and at 323 K. The adsorption was also carried out using CS/SA, and CS/SA/SS and the removal was 44% and 60%, respectively. The adsorption was lower compared to CS/SA/SS/Ben-300 mg. This indicates that crosslinking has a positive impact on the adsorption of MB.

Thermodynamic Modelling

Information on the mechanism and adsorption behaviour of an isothermal system can be determined using adsorption functions such as Gibbs free energy (ΔG°), enthalpy (ΔH°) and entropy (ΔS°) [40]. Equations (4-6) were used to derive thermodynamic parameters such as Gibbs free energy ΔG° , enthalpy (ΔH°), and entropy (ΔS°). These thermodynamic parameters are essential for determining the level of spontaneity.

$$\Delta G^\circ = \Delta H^\circ - T\Delta S^\circ \quad (4)$$

$$\Delta G^\circ = -RT \ln K_d \quad (5)$$

$$\ln K_d = \frac{\Delta S^\circ}{R} - \frac{\Delta H^\circ}{RT} \quad (6)$$

where $K_d = \frac{q_e}{C_e}$, T is the temperature, and R is the universal gas constant. The slope and intercept of Vant Hoff's plot were used to determine both ΔH° and ΔS° . The plot and the thermodynamic parameters are illustrated in Figure 4(a) and Table 1, respectively. The value of ΔG° was negative over the temperature range and increased with temperature, both of which are consistent with the idea that the adsorption of dye on the surface of chitosan beads is spontaneous in nature. The positive value of ΔH° indicates that the adsorption process is endothermic in nature. The positive value of ΔS° reflects that the solid-liquid interface becomes more random after MB adsorption on the beads.

Table 1. Thermodynamic parameters for the adsorption of MB onto CS/SA/SS/Ben composite.

Temperature (K)	q_e (mg/g)	ΔG° (kJ/mol)	ΔH° (kJ/mol)	ΔS° (kJ/mol)	R^2
303	4.58	-2.70	52.62	65.65	0.99
313	4.87	-2.12			
323	5.17	-1.39			

4. Adsorption Kinetics

Information about the adsorption rate, mechanism, and adsorption site distribution can be determined by analysing the experimental data and establishing the adsorption kinetic model. The adopted kinetic models in this study were pseudo-first and second-order kinetic models [41].

The pseudo-first-order model postulates a direct proportionality between the adsorption rate and the number of available adsorption sites on the surface of the adsorbent. The linear pseudo-first-order model is given in equation 7:

$$\ln(q_e - q_t) = \ln q_e - k_1 t \quad (7)$$

where q_e is the equilibrium adsorption capacity, q_t is the amount of adsorbate adsorbed at time t , k_1 is the rate constant of the pseudo-first-order model, and t is the contact time. The q_e and k_1 can be determined from the intercept and slope using the linear fitting equation ($q_e - q_t$) vs t .

The pseudo-second order kinetic model indicates that the rate of adsorption depends on the product of the quantity of adsorbate that is adsorbed at a certain time and the rate constant of the model. This shows that the rate of adsorption is proportional to the amount of adsorbate that is adsorbed at a particular time. The equation for the pseudo second-order model is:

$$\frac{t}{q_e} = \frac{1}{k_2 q_e^2} + \frac{1}{q_e} \quad (8)$$

Where k_2 is the rate constant of the pseudo-second-order model. Fitting the experimental data to

these kinetic models allows for the determination of the rate constants (k_1 and k_2) and the equilibrium adsorption capacity (q_e).

The fitted pseudo-first-order model is shown in Figure 4(b), and the fitted pseudo-second-order model for MB is shown in Figure 4(c). The kinetic model parameters are shown in Table 2. The pseudo-second-order model demonstrates the highest fitting degree ($R^2 = 0.98$), suggesting that the adsorption process is mainly chemisorption.

5. Adsorption Isotherm

The adsorbent-adsorbate interaction and the equilibrium distribution of adsorbate molecules at the solid-liquid phases can be described using adsorption [42]. In this study, the Langmuir and Freundlich Isotherm isotherms were used to describe the adsorption.

The Langmuir isotherm predicts that the adsorption of sorbate from aqueous solution will occur via the construction of a monolayer, and once the monolayer has developed, it will be impossible for any more sorbate to connect to the site that was previously utilised [43],[44]. The Langmuir model is described by equation 9:

$$\frac{C_e}{q_e} = \frac{1}{q_m b} + \frac{C_e}{q_m} \quad (9)$$

where b (mL/mg) and q_m (mg/g) are the Langmuir isotherm constants related to the energy of adsorption and adsorption capacity, respectively. When C_e/q_e was plotted vs C_e , a straight line was obtained. The q_m was calculated from the slope, whereas b was found from the intercept.

Table 2. Kinetic parameters for the removal efficiency of MB by beads composite.

Order of reaction	Parameters	CS/SA/SS/Ben
PFO	$q_{e,exp}$ (mg/g)	3.02
	$q_{e,cal}$ (mg/g)	1.59
	k_1 (min ⁻¹)	4.95×10^{-5}
	R^2	0.283
PSO	$q_{e,cal}$ (mg/g)	3.625
	k_2 (g mg ⁻¹ min ⁻¹)	0.9195
	R^2	0.98

The Freundlich adsorption isotherm predicts that the formation of multilayers on an adsorbent throughout the adsorption process would disclose changes in the surface chemistry of the adsorbent, particle-to-particle contact, and the distribution of sorption heat over the whole surface of the adsorbent [44], [45]. The linear form Freundlich isotherm is expressed by equation 10:

$$\log q_e = \log K_F + \frac{1}{n} \log C_e \quad (10)$$

The following equation displays the adsorption capacity in mg/L and the equilibrium dye concentration in mg/L. The Freundlich isotherm constant and the adsorption intensity are each denoted by the symbols K_F and n , respectively. Empirical methods are used to establish the Freundlich isotherm constants, and these values are very sensitive to variations in a broad variety of environmental variables [46]. The amount

that adsorbs deviate from linearity is directly proportional to the value of its n . When $n = 1$, the adsorption process can be described as linear; when $n < 1$, the adsorption process can be described as chemical; and when $n > 1$, the adsorption process can be described as acceptable [47],[48]. The value of n is calculated to be 0.8 indicating that MB can easily adsorb on the beads. The intercept and slope are two pieces of information that may be used in the calculation of K_F and n . They are obtained by drawing a straight line from $\log q_e$ to $\log C_e$. The fitting of both adsorption models is given in Figure 4(d) and Figure 4(e) and the adsorption parameters are given in Table 3.

The Langmuir isotherm model fits better with $R^2 = 0.99$ compared to the Freundlich model. The maximum monolayer adsorption capacities of optimised adsorbents were found to be 48 mg/g.

Table 3. Isotherm conditions for the removal efficiency of MB by beads composite.

Isotherm	Parameters	CS/SA/SS/Ben
Langmuir	q_{max} (mg/g)	48.94
	K_L (L/mg)	0.0021
	R^2	0.99
Freundlich	K_F (mg/g (L/mg) ^{1/n})	0.1858
	$1/n$	1.2148
	R^2	0.93

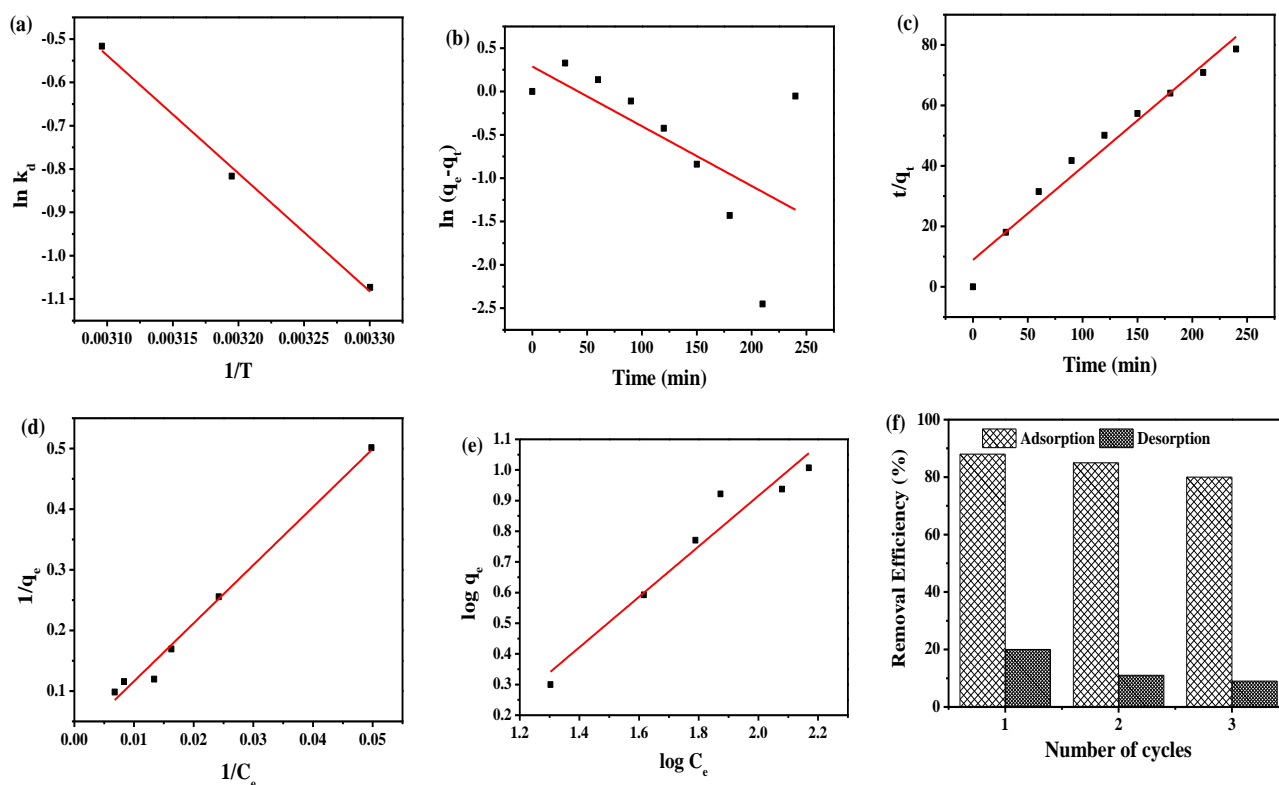


Figure 4. (a) Van't Hoff plot (b) linear plots of pseudo-first-order kinetic model (c) linear plots of pseudo-second-order kinetic model (d) linear plots of the Langmuir isotherm model (e) linear plots of the Freundlich isotherm model and (f) Reusability microsphere at variable number of cycles.

Table 4. Comparative literature survey of chitosan-based adsorbent for MB dye removal.

Adsorbents	Experimental conditions (adsorbent dosage, MB concentration, pH, temperature, time)	Removal efficiency (%)	References
CS/Polyacrylic acid composite	100 mg, 100 mg/L, pH 11, 25 °C, 30 h.	97.74	[49]
CS with hybrid clay nanocomposite	0.015 g, 20 mg/L, pH 7, 30 °C, 24 h.	88	[50]
Activated lignin/CS blend	0.05 g, 50 mg/L, pH 7, 20 °C, 12 h.	88	[51]
CS-montmorillonite/PANI	0.05 g, 100 mg/L, pH 7, 25 °C, 6 h.	82	[43]
CS-epichlorohydrin/zeolite	0.2 g, 100 mg/L, pH 9, 30 °C, 4 h.	90	[44]
Sulfonated CS	50 mg, 100 mg/L, pH 7, 30 °C, 8 h.	95	[45]
CS lignin membrane	1.0 g, 50 mg/L, pH 7, 35 °C, 1 h.	95	[52]
CS/SA/SS/Ben-300 mg	400 mg, 50 mg/L, pH 12, 50 °C, 6 h.	88	Present study

6. Reusability Studies

The CS/SA/SS/Ben-300 mg was repeatedly used for three consecutive cycles and the reusability profile is shown in Figure 4(f). The investigation was carried out under optimum conditions. The desorption of MB from the beads was observed to be less than 20%, indicating that the MB is strongly bonded to the beads. Regardless the adsorption was constant at 82% when reused. The constant adsorption indicates that the beads are highly stable.

Comparison with Reported Adsorbents

Table 4 compares the adsorption potential of CS/SS/SA/Ben-300 mg to the reported chitosan-based adsorbent in the literature. It can be observed that, aside from the performance of the adsorbent materials, the experimental conditions affect dye removal efficiency. Regardless, the comparison shows that CS/SS/SA/Ben-300 mg is equally capable of adsorbing MB. The advantage of the beads compared to other adsorbents is that they can be easily separated and reused due to the bigger size of the beads.

CONCLUSION

The analyses indicate that CS/SA/SS/Ben-300 mg could adsorb 88% of MB under the optimum conditions (400 mg of beads, initial MB concentration of 50 mg/L MB at pH 12 for 6 h and at 323 K). The adsorption of MB using CH/SA, and CH/SA/SS was 44% and 60%, respectively. The increase is due to the presence of various adsorption sites as the result of crosslinking of all the components. The adsorption potential of CS/SA/SS/Ben-300 mg was compared to other chitosan-modified adsorbents reported in the literature. In addition to having comparable adsorption capacity, the advantage of the beads is that they can easily be separated and reused due to the bigger size of the beads.

ACKNOWLEDGEMENTS

This research was funded by the Ministry of Education Malaysia (Higher Education) for the Fundamental Research Grant Scheme (FRGS/1/2023/STG01/USM/02/2).

REFERENCES

1. Yaqoob, A. A., Parveen, T., Umar, K. and Mohamad Ibrahim, M. N. (2020) Role of nanomaterials in the treatment of wastewater: a review. *Water*, **12**(2), 495.
2. Kausar, A., *et al.* (2019) Preparation and characterization of chitosan/clay composite for direct Rose FRN dye removal from aqueous media: comparison of linear and non-linear regression methods. *Journal of Materials Research and Technology*, **8**(1), 1161–1174.
3. Pang, Y. L. and Abdullah, A. Z. (2013) Current status of textile industry wastewater management and research progress in Malaysia: a review. *CLEAN Soil Air Water*, **41**(8), 751–764.
4. Idris, M. O., Kim, H. -C., Yaqoob, A. A. and Ibrahim, M. N. M. (2022) Exploring the effectiveness of microbial fuel cell for the degradation of organic pollutants coupled with bio-energy generation. *Sustainable Energy Technologies and Assessments*, **52**, 102183.
5. Isari, A. A., Payan, A., Fattahi, M., Jorfi, S. and Kakavandi, B. (2018) Photocatalytic degradation of rhodamine B and real textile wastewater using Fe-doped TiO₂ anchored on reduced graphene oxide (Fe-TiO₂/rGO): Characterization and feasibility, mechanism and pathway studies. *Applied Surface Science*, **462**, 549–564.

6. Idris, M. O., Yaqoob, A. A., Ibrahim, M. N. M., Ahmad, A. and Alshammari M. B. (2023) Introduction of adsorption techniques for heavy metals remediation. *Emerging Techniques for Treatment of Toxic Metals from Wastewater*, 1–18.
7. Hamad, H. N. and Idrus, S. (2022) Recent developments in the application of bio-waste-derived adsorbents for the removal of methylene blue from wastewater: a review. *Polymers*, **14**(4), 783.
8. Kayiwa, R., Kasedde, H., Lubwama, M. and Kirabira, J. B. (2021) The potential for commercial scale production and application of activated carbon from cassava peels in Africa: A review. *Bioresource Technology Reports*, **15**, 100772.
9. Şahin, Ö., Kaya, M. and Saka, C. (2015) Plasma-surface modification on bentonite clay to improve the performance of adsorption of methylene blue. *Applied Clay Science*, **116–117**, 46–53.
10. Shahinpour, A., Tanhaei, B., Ayati, A., Beiki, H. and Sillanpää, M. (2022) Binary dyes adsorption onto novel designed magnetic clay-biopolymer hydrogel involves characterization and adsorption performance: Kinetic, equilibrium, thermodynamic, and adsorption mechanism. *Journal of Molecular Liquids*, **366**, 20303.
11. Marrakchi, F., Hameed, B. H. and Hummadi, E. H. (2020) Mesoporous biohybrid epichlorohydrin crosslinked chitosan/carbon–clay adsorbent for effective cationic and anionic dyes adsorption. *International Journal of Biological Macromolecules*, **163**, 1079–1086.
12. Khan, M. N., Chowdhury, M. and Rahman, M. M. (2021) Biobased amphoteric aerogel derived from amine-modified clay-enriched chitosan/alginate for adsorption of organic dyes and chromium(VI) ions from aqueous solution. *Materials Today Sustainability*, **13**, 100077.
13. Aksu Demirezen, D., Demirezen Yılmaz, D. and Yıldız, Y. Ş. () Magnetic chitosan/calcium alginate double-network hydrogel beads: Preparation, adsorption of anionic and cationic surfactants, and reuse in the removal of methylene blue. *International Journal of Biological Macromolecules*, **239**, 124311.
14. Saheed, I. O., Oh, W. D. and Suah, F. B. M. (2021) Chitosan modifications for adsorption of pollutants – A review. *Journal of Hazardous Materials*, **408**, 124889.
15. Kang, S., Park, S. -M., Park, J. -G. and Baek, K. (2019) Enhanced adsorption of arsenic using calcined alginate bead containing alum sludge from water treatment facilities. *Journal of Environmental Management*, **234**, 181–188.
16. Khanday, W. A., Asif, M. and Hameed, B. H. (2016) Cross-linked beads of activated oil palm ash zeolite/chitosan composite as a bio-adsorbent for the removal of methylene blue and acid blue 29 dyes. *International Journal of Biological Macromolecules*, **95**, 895–902.
17. Oussalah, A. and Boukerroui, A. (2020) Alginate-bentonite beads for efficient adsorption of methylene blue dye. *Euro-Mediterranean Journal for Environmental Integration*, **5**(2), 31.
18. Al-Remawi, M. M. A. (2012) Properties of Chitosan Nanoparticles Formed Using Sulfate Anions as Crosslinking Bridges. *American Journal of Applied Sciences*, **9**(7) 1091–1100.
19. Zhu, R., Zhu, L., Zhu, J., Ge, F. and Wang, T. (2009) Sorption of naphthalene and phosphate to the CTMAB–Al13 intercalated bentonites. *Journal of Hazardous Materials*, **168**(2–3) 1590–1594.
20. Yang, L., et al. (2021) Floating chitosan-alginate microspheres loaded with chlorantraniliprole effectively control *Chilo suppressalis* (Walker) and *Sesamia inferens* (Walker) in rice fields. *Science of The Total Environment*, **783**, 147088.
21. Kuczajowska-Zadrożna, M., Filipkowska, U. and Józwiak, T. (2020) Adsorption of Cu(II) and Cd(II) from aqueous solutions by chitosan immobilized in alginate beads. *Journal of Environmental Chemical Engineering*, **8**(4), 103878.
22. Ahmad, R. and Ansari, K. (2021) Comparative study for adsorption of congo red and methylene blue dye on chitosan modified hybrid nanocomposite. *Process Biochemistry*, **108**, 90–102.
23. Abdul Mubarak, N. S., Bahrudin, N. N., Jawad, A. H., Hameed, B. H. and Sabar, S. (2021) Microwave enhanced synthesis of sulfonated chitosan-montmorillonite for effective removal of methylene blue. *Journal of Polymers and the Environment*, **29**(12), 4027–4039.
24. Kiefer, J., Stärk, A., Kiefer, A. and Glade, H. (2018) Infrared spectroscopic analysis of the inorganic deposits from water in domestic and technical heat exchangers. *Energies*, **11**(4), 798.
25. Dehghani, M. H., et al. (), Production and application of a treated bentonite–chitosan composite for the efficient removal of humic acid from aqueous solution. *Chemical Engineering Research and Design*, **140**, 102–115.
26. Da Silva, J. C. S., et al. (2021) What happens when chitosan meets bentonite under microwave-

- assisted conditions? Clay-based hybrid nanocomposites for dye adsorption. *Colloids and Surfaces A: Physicochemical and Engineering Aspects*, **609**, 125584.
27. Annan, E., Arkorful, G. K., Konadu, D. S., Asimeng, B., Dodoo-Arhin, D. and Eglewogbe, M. (2021) Synthesis and characterization of hydroxyapatite- (HAP-) clay composites and adsorption studies on methylene blue for water treatment. *Journal of Chemistry*, 1–15.
28. Fabia, J., Janicki, J., Ślusarczyk, C., Rom, M., Graczyk, T. and Gawłowski, A. (2015) Study of structure of polypropylene microfibrils modified with multi-walled carbon nanotubes. *F&TInEE*, **23**, **3(111)**, 38–44.
29. Govindan, S., Nivethaa, E. A. K., Saravanan, R., Narayanan, V. and Stephen, A. () Synthesis and characterization of chitosan–silver nanocomposite. *Applied Nanoscience*, **2(3)**, 299–303.
30. Saeedi Garakani, S., *et al.* (2020) Fabrication of chitosan/polyvinylpyrrolidone hydrogel scaffolds containing PLGA microparticles loaded with dexamethasone for biomedical applications. *International Journal of Biological Macromolecules*, **164**, 356–370.
31. Zhang, X. and Sun, J. (2020) Synthesis, Characterization, and properties of sulfonated chitosan for protein adsorption. *International Journal of Polymer Science*, 2020, 1–10.
32. Sharifpour, E., Alipanahpour Dil, E., Asfaram, A., Ghaedi, M. and Goudarzi, A. () Optimizing adsorptive removal of malachite green and methyl orange dyes from simulated wastew 22 by Mn-doped CuO-nanoparticles loaded ... activated carbon using CCD-RSM: Mechanism, regeneration, isotherm, kinetic, and thermodynamic studies. *Applied Organometallic Chemistry*, **33(3)**, e4768.
33. Kurczewska, J. (2022) Chitosan-montmorillonite hydrogel beads for effective dye adsorption. *Journal of Water Process Engineering*, **48**, 102928.
34. Bayomie, O. S., Kandeel, H., Shoeib, T., Yang, H., Youssef, N. and El-Sayed, M. M. H. () Novel approach for effective removal of methylene blue dye from water using fava bean peel waste. *Scientific Reports*, **10(1)**, 7824.
35. Hashem, A. H., Saied, E. and Hasanin, M. S. (2020) Green and ecofriendly bio-removal of methylene blue dye from aqueous solution using biologically activated banana peel waste. *Sustainable Chemistry and Pharmacy*, **18**, 100333.
36. Ablouh, E., Hanani, Z., Eladlani, N., Rhazi, M. and Taourirte, M. (2019) Chitosan microspheres/sodium alginate hybrid beads: an efficient green adsorbent for heavy metals removal from aqueous solutions. *Sustainable Environment Research*, **29(1)**, 5.
37. Naeem, S., Baheti, V., Wiener, J. and Marek, J. () Removal of methylene blue from aqueous media using activated carbon web. *The Journal of The Textile Institute*, **108(5)**, 803–811.
38. Fu, J. *et al.*, (2015) Adsorption of methylene blue by a high-efficiency adsorbent (polydopamine microspheres): Kinetics, isotherm, thermodynamics and mechanism analysis. *Chemical Engineering Journal*, **259**, 53–61.
39. Meng, B., Guo, Q., Men, X., Ren, S., Jin, W. and Shen, B. (2020) Modified bentonite by polyhedral oligomeric silsesquioxane and quaternary ammonium salt and adsorption characteristics for dye. *Journal of Saudi Chemical Society*, **24(3)**, 334–344.
40. Jawad, A. H., *et al.* (2017) Microwave-assisted preparation of mesoporous-activated carbon from coconut (*Cocos nucifera*) leaf by H₃PO₄ activation for methylene blue adsorption. *Chemical Engineering Communications*, **204(10)**, 1143–1156.
41. Zhao, S., *et al.* (2023) Efficient adsorption of methylene blue in water by nitro-functionalized metal-organic skeleton-calcium alginate composite aerogel. *International Journal of Biological Macromolecules*, **253**, 126458.
42. Njoku, V. O., Foo, K. Y., Asif, M. and Hameed, B. H. (2014) Preparation of activated carbons from rambutan (*Nephelium lappaceum*) peel by microwave-induced KOH activation for acid yellow 17 dye adsorption. *Chemical Engineering Journal*, **250**, 198–204.
43. Foo, K. Y. and Hameed, B. H. (2010) Insights into the modeling of adsorption isotherm systems. *Chemical Engineering Journal*, **156(1)**, 2–10.
44. Ayawei, N., Ebelegi, A. N. and Wankasi, D. (2017) Modelling and interpretation of adsorption isotherms. *Journal of Chemistry*, 2017, 1–11.
45. Mozaffari Majd, M., Kordzadeh-Kermani, V., Ghalandari, V., Askari, A. and Sillanpää, M. (2022) Adsorption isotherm models: A comprehensive and systematic review (2010–2020). *Science of The Total Environment*, **812**, 151334.
46. Rangabhashiyam, S., Anu, N., Giri Nandagopal, M. S. and Selvaraju, N. (2014) Relevance of isotherm models in biosorption of pollutants by agricultural byproducts. *Journal of Environmental Chemical Engineering*, **2(1)**, 398–414.

47. Salleh, M. A. M., Mahmoud, D. K., Karim, W. A. W. A. and Idris, A. (2011) Cationic and anionic dye adsorption by agricultural solid wastes: A comprehensive review. *Desalination*, **280**(1–3), 1–13.
48. Batool, F., Akbar, J., Iqbal, S., Noreen, S. and Bukhari, S. N. A. (2018) Study of isothermal, kinetic, and thermodynamic parameters for adsorption of cadmium: an overview of linear and nonlinear approach and error analysis. *Bioinorganic Chemistry and Applications*, 2018, 1–11.
49. Zheng, X., Bi, C., Li, Z., Podariu, M. and Hage, D. S. (2015) Analytical methods for kinetic studies of biological interactions: A review. *Journal of Pharmaceutical and Biomedical Analysis*, **113**, 163–180.
50. Revellame, E. D., Fortela, D. L., Sharp, W., Hernandez, R. and Zappi, M. E. () Adsorption kinetic modeling using pseudo-first order and pseudo-second order rate laws: A review. *Cleaner Engineering and Technology*, **1**, 100032.
51. Ho, Y. (2006) Review of second-order models for adsorption systems. *Journal of Hazardous Materials*, **136**(3), 681–689.
52. Roostaei, N. and Tezel, F. H. (2004) Removal of phenol from aqueous solutions by adsorption. *Journal of Environmental Management*, **70**(2), 157–164.